Interaction of a vortex ring with a natural convective layer

C. Palacios-Morales, G. Gelderblom, F. Solorio, M. Salinas-Vázquez, and R. Zenit

Citation: Physics of Fluids (1994-present) **26**, 083602 (2014); doi: 10.1063/1.4891985
View online: http://dx.doi.org/10.1063/1.4891985
View Table of Contents: http://scitation.aip.org/content/aip/journal/pof2/26/8?ver=pdfcov
Published by the AIP Publishing

PHYSICS OF FLUIDS **26**, 083602 (2014)

Interaction of a vortex ring with a natural convective layer

C. Palacios-Morales,[1] G. Gelderblom,[2,3] F. Solorio,[1] M. Salinas-Vázquez,[4] and R. Zenit[2]

[1]*Facultad de Ingeniería, Universidad Nacional Autónoma de México, Ciudad Universitaria, 04510, Mexico, D.F.*

[2]*Instituto de Investigaciones en Materiales, Universidad Nacional Autónoma de México, Ciudad Universitaria, 04510, Mexico, D.F.*

[3]*University of Twente, P.O. Box 217, 7500 AE Enschede, The Netherlands*

[4]*Instituto de Ingeniería, Universidad Nacional Autónoma de México, Ciudad Universitaria, 04510, Mexico, D.F.*

(Received 25 October 2013; accepted 21 July 2014; published online 12 August 2014)

We study the dynamics of the interaction of a vortex ring with a shear flow, generated by a natural convective layer. Laminar vortex rings were generated in water with a piston-cylinder arrangement. To generate the shear flow, a vertical wall was heated by a thermal bath held at constant temperature to produce a laminar and stable thermal boundary layer with a Grashof number of O(10^8). Measurements of the two-dimensional velocity field were obtained with a time resolved particle image velocimetry technique. Additionally, a 3D numerical model was used to simulate the experimental conditions. We mainly conducted experiments for the piston stroke $L/D_0 = 1$ and Re of O(1000). The velocity ratio $r = U_{vi}/U_{sh}$ (where U_{vi} is the initial vortex velocity and U_{sh} is the maximum velocity of the shear layer) was in the range $2.2 \leq r \leq 3.6$. The results show that as the vortex approaches the shear layer, the ring expands and stretches mainly in the vertical direction and tilts slightly forming an angle between the wall and the ring plane which increases to about 3°. The rate of reduction of circulation is slower at the lower section of the vortex ring indicating that the momentum transport is more significant in this region. Moreover, the vortex circulation at the lower section increases to about 20% compared to the isothermal case. An analysis of the different mechanisms leading to this ring-shear layer interaction is presented and comparisons with reported data are discussed. [http://dx.doi.org/10.1063/1.4891985]

I. INTRODUCTION

The study of convective heat transfer is very important due its relevance in many engineering applications such as combustion, electronic cooling devices, and heat exchangers. Many works are focused on improving the design of different heat transfer devices; particularly, researchers have made efforts to understand the interaction between fluid flow and solid walls to enhance the rate of heat transfer. Researchers have drawn attention to the study of the heat transfer in walls in the presence of turbulent flows.[1,2] Recent studies indicate that turbulence is not just a chaotic motion of fluid but it is composed by well defined vortical structures that interact with the wall surface.[3] The role of vortical structures and its implications to increase the heat transfer has been studied by different authors.[4,5] In fact, different techniques are used to generate these vortices artificially in the flow in order to enhance wall heat transfer.[6,7] The heat transfer resulting from the interaction of individual vortices with heated walls has been studied in recent years.[8,9] In a numerical study, Martin and Zenit[9] showed that as a vortex pair approached the wall, a volume of heated fluid is convected from the surface increasing significantly the heat transfer. Recently, different experimental works have studied the collision of single vortex rings with vertical heated walls.[10–12] Arévalo *et al.*[10] studied the interaction of a vortex ring in air in collision with a vertical heated wall, their results indicated that there was an increment of the heat transfer as a result of the impact which increases with the vortex

Reynolds number. Later, Arévalo *et al.*[11] expanded their study and conducted measurements with the particle image velocimetry (PIV) technique to show that the vorticity and shear stresses are the basic ingredients to enhance the heat transfer. More recently, Hubble *et al.*[12] studied the interaction of a vortex ring with a heated wall in water. They showed that the heat transfer augmentation is greatly influenced by the force, size, and position of the vortex ring relative to the thermal boundary layer generated by free-convection.

Vortex rings have been studied for more than a century[13–15] because they represent a canonical flow in fluid mechanics. The reason to work with this kind of vortices is because they are very reproducible in laboratory and some properties such as the vortex size and travel velocity can be easily controlled. The dynamics of the interaction of vortex rings with solid walls and bodies has been addressed as well.[16] The seminal paper of Walker and Smith[17] studied the dynamics of the impact of a vortex ring approaching to a solid flat wall in a trajectory normal to the wall. The main characteristics of the collision were studied by ink visualizations. As the ring approaches to the wall the vortex diameter increases symmetrically, the vortex induces an unsteady separation of the boundary layer and, depending on the vortex strength, the generation of secondary and tertiary vortices were observed. Also, depending on the vortex Reynolds number azimuthal waves or instabilities develop from the secondary vortex. These main characteristics were confirmed numerically by Orlandi and Verzicco.[18] Subsequent works have provided information about the vortex stretching, kinetic energy, pressure gradients, and surface force during collision.[19–21]

The dynamics of the interaction of the vortex ring with the natural convective layer generated by a vertical heated wall has not been studied in detail. It has been observed that the vortex ring expands asymmetrically during collision and the thickness of the ring becomes non-uniform as it propagates into the flow;[10] therefore, the details of this phenomenon have to be fully understood. Different authors have studied the interaction of single vortex rings in crossflows.[22–25] Depending on the velocity ratio (initial vortex velocity to free stream crossflow velocity), the vortex ring may tilt and deform as it propagates downstream. If the vortex velocity is large enough, the ring tilts towards the upstream direction[23] up to 30° depending also on the ring strength.[22] The vortex ring rotation may be influenced by the nature of the stream which may be a shear or uniform flow.[24] Cheng *et al.*[25] attributed this behavior to the modification of vorticity distribution of the vortex ring as a result of the entrainment of background vorticity. Recently, Guzmán *et al.*[26] studied numerically the interaction of a dipolar vortex with a shear layer generated by a sliding vertical wall, obtaining similar results.

The objective of this paper is to study, by experiments and numerical simulations, the collision of a vortex ring shear flow, resulting from the natural convection of a heated wall. A 3D numerical model is used to simulate both a vertical heated wall kept at constant temperature and a single vortex ring traveling in a normal trajectory to the wall. The results from this model are compared with experimental measurements using piston-cylinder arrangement and a time resolved PIV (TR-PIV) technique. The aim of this first study is not yet to study the heat transfer; the focus of this paper is on the dynamics of the vortex ring approaching the wall and its interaction with the heat-induced convection layer near the wall. Different wall temperatures, Reynolds numbers, and piston stroke ratios are considered. Previous works[10–12] have shown that the interaction of the vortex ring and the thermal boundary layer generates an asymmetric expansion of the ring. We will show that this asymmetry is also observed in the trajectory of the vortex ring during collision. Moreover, the circulation of the vortex ring during collision depends on the vortex section position relative to the thermal boundary layer. This paper is organized as follows. In Secs. I and I A, we first show a brief description and a background of the problem. Section II describes the experimental setup and measurements while Sec. III explains the numerical method. The flow properties are presented in Sec. IV. The characteristics of the ring-wall collision are studied in detail in Sec. V. Concluding remarks are summarized in Sec. VI.

A. Problem statement and background

In this investigation, the interaction of a vortex ring with a heated wall is studied. Particularly, we focus on evaluating the flow dynamics of the vortex ring with the shear flow created by natural

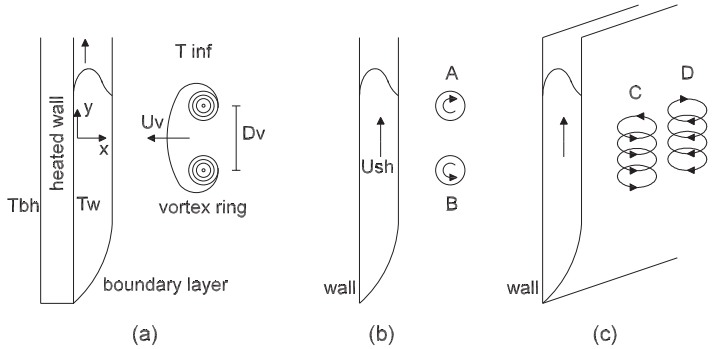

FIG. 1. (a) Parameters, (b) vertical regions, (c) horizontal regions: The interaction of a vortex ring with a vertical heated wall.

convection. The problem under investigation is showed schematically in Fig. 1(a). A vortex ring with diameter D_v and translation velocity U_v moves in a trajectory perpendicular to a vertical heated wall (y-direction). The solid wall is kept at a constant temperature T_w. A boundary layer of thickness $\delta(y)$ and velocity $U_{sh}(x, y)$ is generated at the vicinity of the wall. The axis x coincides with the axial axis of the ring and the wall is located in the plane $x = 0$. The ring diameter and translation velocity change slightly during vortex motion; in particular, U_{vi} represents the initial vortex velocity, i.e., the velocity after ring formation, which is also the maximum vortex velocity. The fluid and the walls, with the exception of the heated plate, are initially at the same temperature T_{inf}. When the vortex ring reaches the boundary layer, a complex 3D behavior is observed. To make a description as clear as possible we consider four different regions of the ring and analyze their evolution in time. The principal vortex regions of the vortex ring are shown in Figs. 1(b) and 1(c). Vortex sections A and B can be obtained considering a vertical slice of the ring. The upper section A of the vortex ring rotates in the same direction as the outer region of the boundary layer flow. The lower (bottom) section B has a spin in a direction opposite to that of the boundary flow. Lateral sections C and D are obtained considering a horizontal slice of the ring. For sections A and B, the normal vorticity ω_z is parallel to the normal vorticity of the main flow of the boundary layer. On the other hand, the two side regions C and D have vorticity, ω_y, which is perpendicular to the vorticity of the layer.

The Reynolds number for vortex rings has been defined in different forms. A common definition[27] is $Re = \Gamma/\nu$, where Γ is the vortex ring circulation and ν is the kinematic viscosity of the fluid. In other terms, the Reynolds number can also be defined as[11] $Re = D_v U_v/\nu$. As we will show in this paper, the travel vortex velocity as well as the circulation may decrease slightly during vortex propagation for relatively small piston strokes and long travel distances. Considering parameters from the piston-cylinder arrangement (see Fig. 2) and following Rosenfeld *et al.*,[28] we

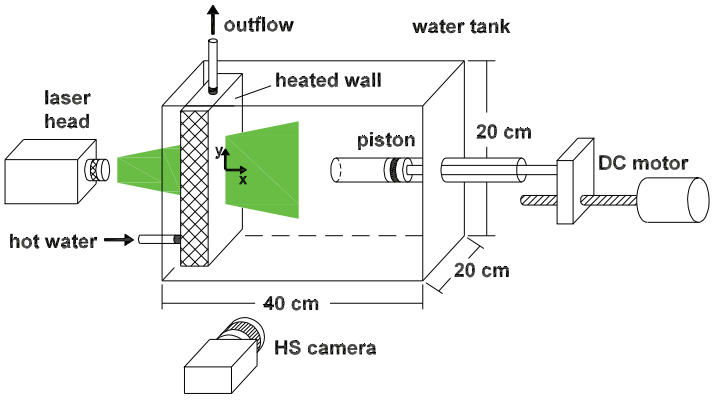

FIG. 2. Experimental setup.

define the Reynolds number as $Re = D_0 U_{p,\,max}/\nu$, where D_0 is the cylinder inner (or exit nozzle) diameter and $U_{p,\,max}$ is the maximum piston velocity. The mean piston velocity U_p is defined as

$$U_p = \frac{1}{t_p}\int_0^{t_p} u_p(t)dt, \tag{1}$$

where $u_p(t)$ is the history of the piston velocity and t_p is the discharge time. The piston stroke ratio was defined as $L/D_0 = U_p t_p/D_0$ where L is the total piston displacement or piston stroke. To study the evolution of the vortex ring, the time was scaled with the tube diameter and the initial vortex translation velocity $t* = tU_{vi}/D_0$. In all cases, the piston motion starts at $t = 0$. We conducted experiments for piston stroke ratios $1 \leq L/D_0 \leq 3$, the range of piston velocities was $7 \leq U_{p,\,max} \leq 15$ cm/s, and the resulting Reynolds numbers were $1360 \leq Re \leq 2910$. The range of temperature differences studied experimentally (and numerically) were $\Delta T = T_w - T_{inf} = 7.6, 12.8, 18\,^{\circ}\mathrm{C}$.

The position of the vortex centers was obtained by the computation of the curvature of Lagrangian trajectories, i.e., the trajectories of individual moving fluid elements.[29] In regions where the local velocity becomes zero (vortex centers), the direction of fluid particles changes over very short length scales, producing large curvature values. The curvature was computed by the formula proposed by Braun *et al.*[30]

$$k(t) = \frac{|\boldsymbol{u} \times \partial_t \boldsymbol{u} + \boldsymbol{u} \times [\boldsymbol{u} \cdot \nabla \boldsymbol{u}]|}{|\boldsymbol{u}|^3}, \tag{2}$$

where $\boldsymbol{u}$ is the velocity field. To measure the vortex ring circulation, we first obtained the vortex ring area on the measurement plane. Different schemes based on local analysis of the velocity gradient tensor $\nabla \boldsymbol{u}$ have been used to identify vortex rings.[31] In this investigation, we used the position of the vortex center and the Q criterion method to identify the vortex core region and compute its circulation. The Q criterion of Hunt *et al.*[32] for an incompressible flow ($\nabla \cdot \boldsymbol{u} = 0$) is defined as

$$Q = \frac{1}{2}(|\Omega|^2 - |D|^2), \tag{3}$$

where Ω is the vorticity tensor and D is the rate of strain tensor. In regions where $Q > 0$, the local measure of rotation rate is larger than the strain rate; therefore, the spatial region belongs to a vortex. Detailed information of this technique can be found elsewhere.[33] In our case, we define the vortex rings as the regions where $Q > 0.01\ \mathrm{s}^{-2}$. The circulation is calculated from

$$\Gamma = \int_{A_Q} \omega_z dA, \tag{4}$$

where ω_z is the azimuthal vorticity and A_Q is the vortex region.

II. EXPERIMENTAL SETUP

The vortex rings were generated using a piston-cylinder apparatus which is schematically represented in Fig. 2. Vortex formation was obtained by pushing a volume of fluid out of a horizontal tube with free end in a tank filled of water. The tank dimensions were 40 × 20 × 20 cm and the cylinder inner diameter was $D_0 = 1.94$ cm. The cylinder was 40 cm long, it was placed 10 cm from the base wall and 8 cm from the lateral wall (wall-cylinder coupling); both the tank and tube are made of glass. The tube outer wall is sharp-edged at the exit with a tip angle of 20° in order to avoid edge effects on the vortex formation. The piston was connected to a sledge which was driven through a screw to a DC motor. The motor is a BALDOR DC Gear motor with 1/25 HP and 90 V – 0.5 A maximum. It produces 5.1 lb s of torque and output velocity of approximately 1700 rpm without gear reducer. The motor was driven by a computer controlled power supply; specifically, we controlled the piston velocity $u_p(t)$ introducing a fixed voltage, the current, and feed time. The mean piston velocity is proportional to the voltage supplied by the motor. For relatively small piston velocities and large stroke ratios $L/D_0 \geq 4$, the piston velocity program is mainly impulsive; however, for small piston strokes the acceleration and deceleration stages are important.

A vertical wall heated at a constant temperature was used to study the ring-wall interaction. A schematic overview of the system is shown in Fig. 2. The vertical wall (17.5 × 19.5 cm) is made of glass with 3 mm of thickness and was built-in a water-tight vertical box. The temperature at the wall surface is kept constant by means of a water bath (Thermo Haake k15 and a circulator DC10). A constant water flow, with temperature T_{bh}, was driven inside this "heating-box"; the inflow and outflow were set at the bottom and top walls, respectively. The system has 17 l/min circulation capacity, an operating temperature range from −30 to 100 °C and a temperature accuracy of 0.02 ± °C. The outer heating-box dimensions are 17.5 × 19.5 × 4 cm, all the walls are made of Plexiglas with 12 mm thickness and were covered by cork paper (3 mm) as a thermal isolating material. The distance from the tube exit to the vertical wall is the range of 135–184 mm. Temperature measurements tests (before ring-wall experiments) were made on the wall surface using thermocouples placed along the vertical direction. Measurements were done using fast response surface thermocouples SA1 series J type of Omega Engineering. The dimensions of the sensor pad are 19 × 25 × 0.3 mm and has self-adhesive backing, the temperature rating is −60 °C–177 °C and the sensor has 0.3 s response time.

In the present study, we obtain the two-dimensional (2D) (vertical) velocity field perpendicular to the wall using a time resolved PIV system. Further details on the PIV technique can be found in Refs. 34 and 35. The PIV system consists of a Nd:YAG Litron laser (532 nm, 10 mJ, 1000 Hz), a Phantom high speed camera (1632 × 1200 pixels, 11.5 μm pixel pitch, 1000 Hz), and a Dantec Dynamics PIV software. Neutrally buoyant silver-coated glass spheres with an average diameter 10 μm were used as particle tracers. The laser sheet illuminated a vertical slice aligned with the tube center. On the rear wall of the vertical box there was a vertical gap (without insulation material) whereby the laser beam passed through as shown in Fig. 2. A typical measurement area was 120 × 180 mm. The velocity field consisted of 147 × 201 vectors using an interrogation area of 32 × 32 pixels with an overlap of 75% with a spatial resolution of 0.88 mm. For the ring-wall collision experiments the sampling rate was 100 Hz.

Since one of the aims of the present study is to draw direct comparisons between experiments and numerical simulations, the uncertainty of the PIV system must be assessed. This particular issue is actively being discussed in the community and several approaches can be followed (see Refs. 36 and 37 for recent discussions). Based on our previous work,[33] we determined an uncertainty of roughly 6% in all measurements.

In Fig. 3(a), we show the piston velocity program $u_p(t)$ (obtained experimentally) for a stroke ratio $L/D_0 = 1$ and a feed voltage of 60 V. We measured the piston velocity by calculating its displacement between consecutive frames obtained from the high speed camera (100 Hz) described above. In this case, the discharge time is $t_p = 0.4$ s, the maximum piston velocity is $U_{p,\,max} = 12$ cm/s,

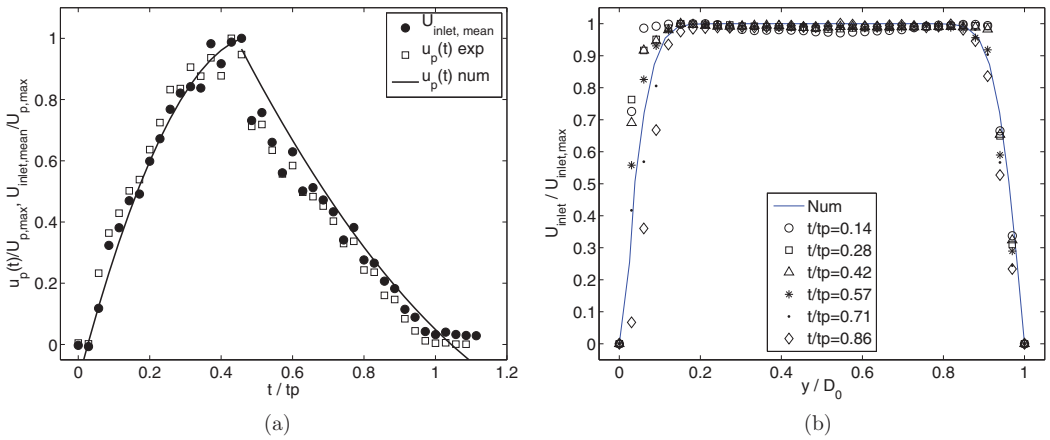

FIG. 3. (a) Piston velocity program $u_p(t)$ and mean inlet velocity (inside tube) $U_{inlet,\,mean}$, the lines correspond to an approximation of $u_p(t)$ for numerical simulations. (b) Inlet velocity profile obtained from PIV measurements and the approximation function for numerical simulations.

and the mean piston velocity is $U_p \approx 5.3$ cm/s, obtained from Eq. (1). In order to have similar initial conditions, we obtained two approximation functions of the form $u_p(t) = a + bt + ct^2$ to impose an artificial piston velocity $u_p(t)$ (num) program in the numerical model, which are also plotted in this figure. In Fig. 3(b), we show the inlet velocity profile obtained from PIV measurements inside the cylinder for the same piston velocity and piston stroke shown in Fig. 3(a); the velocity profiles were measured at a distance of 5 mm from the tube exit. For this particular Reynolds number ($Re = 2328$), we observe that the velocity profile at the center of the tube is flat. The mean inlet velocity $U_{inlet,\,mean}$ obtained from these profiles is plotted in Fig. 3(a). We can observe that both piston velocity $u_p(t)$ and mean inlet velocity $U_{inlet,\,mean}$ coincide.

III. NUMERICAL METHOD

A. Flow equations

In a Cartesian frame of reference x, y, z, the Navier-Stokes equations can be written as an extension of the following compressible equations:[38]

$$\frac{\partial \boldsymbol{U}}{\partial t} + \frac{\partial \boldsymbol{F_i}}{\partial x_i} = \boldsymbol{S_F}, \tag{5}$$

where $\boldsymbol{U}$ is a four component vector defined by

$$\boldsymbol{U} = (\rho, \rho u, \rho v, \rho w), \tag{6}$$

where ρ is the fluid density. Equations (5) and (6) represent the evolution of the density (continuity equation) and momentum. The velocity vector $\boldsymbol{u} = (u_1, u_2, u_3)$ is also written as $\boldsymbol{u} = (u, v, w)$. $\boldsymbol{F_i}$ are the fluxes, where $\forall i \in \{1, 2, 3\}$, this is given by

$$\boldsymbol{F_i} = \begin{pmatrix} \rho u_i \\ \rho u_i u_1 + p\delta_{i1} - 2\mu S_{i1} \\ \rho u_i u_2 + p\delta_{i2} - 2\mu S_{i2} \\ \rho u_i u_3 + p\delta_{i3} - 2\mu S_{i3} \end{pmatrix}, \tag{7}$$

where μ is the fluid viscosity, δ_{ij} symbol is the Kronecker delta, whereas $\boldsymbol{S_{ij}}$ is the deviatoric part of the deformation tensor, which is written as

$$\boldsymbol{S_{ij}} = \frac{1}{2}\left(\frac{\partial u_i}{\partial x_j} + \frac{\partial u_j}{\partial x_i} - \frac{2}{3}(\nabla \cdot \boldsymbol{u})\right). \tag{8}$$

Instead of using the artificial continuity equation (artificial compressibility approach[39]) herein, the pressure is replaced in the compressible Navier-Stokes equation according with the equation of state for an artificial incompressible fluid[40]

$$p = \rho c^2, \tag{9}$$

where c is the speed of sound of the fluid, p is the pressure, and ρ is the considered density. As long as the Mach number of the flow decreases ($M < 0.1$) and the conditions become almost isothermal, the solution to this set of equations should approach the incompressible limit. Finally, the term $\boldsymbol{S_F}$ corresponds to a forcing term in order to reproduce the gravitational effect (incompressible approximation)

$$\begin{aligned} \boldsymbol{S_F} &= (S_\rho, S_{\rho u}, S_{\rho v}, S_{\rho w}), \\ S_\rho &= S_{\rho u} = S_{\rho w} = 0, \\ S_{\rho v} &= \frac{\beta \Delta T}{(Fr)^2}, \end{aligned} \tag{10}$$

where β is the volumetric thermal expansion of the fluid and Fr is the Froude number. For simplicity purposes, the notation was changed in the section dedicated to show our results. In particular, both

velocity and space direction vectors were changed from (u_1, u_2, u_3) to (u, v, w) and from (x_1, x_2, x_3) to (x, y, z), respectively. Also, the x-direction corresponds to the streamwise direction, z-direction to the spanwise direction, and y-direction represents the normal direction.

B. Large eddy simulation (LES)

Turbulent effects throughout the flow field were simulated with the LES algorithm, consisting of a deterministic simulation of the characteristic large scales along the flow, which are considered to be the most energetic. According to Lesieur and Métais,[41] small scales should be filtered since kinetic energy is transferred between the latter and the large scales, thus influencing the large scale momentum. Therefore, the small scales effect was included into the present model from the selective structure function model.[42] Turbulent thermal conductivity is obtained from constant turbulent Prandtl number, equal to 0.6. No extra terms were added to the sub-grid model due to the natural convection.

C. Numerical resolution

The generalized coordinate system is solved by extension of the fully explicit McCormack scheme, second order in time and fourth order in space, developed by Gottlieb and Turkel.[43] This code has been validated and widely used in different flows.[38,44,45] The inlet boundary condition used herein is that proposed by Poinsot and Lele.[46] At the inlet boundary condition, we impose two different streamwise velocity profiles. A smoothed "top-hat" function (Mohseni *et al.*[47])

$$u_{inlet}(r) = max(0.0, \boldsymbol{erfc}(\epsilon(r - R)) - 1.0), \tag{11}$$

where R is the total nozzle radius, r the radial coordinate from the nozzle center, $\boldsymbol{erfc}$ is the error function, and ϵ is a parameter that controls the smoothing of the profile and it is a reminiscent of the boundary layer thickness at the exit of the nozzle in experiment. The second profile considers a laminar pipe flow at the exit of the nozzle[48]

$$u_{inlet}(r) = max\left(0.0, u_{inlet,max}\left(1.0 - \left(\frac{r^2}{R^2}\right)\right)\right), \tag{12}$$

where $u_{inlet,\,max}$ is the maximal nozzle velocity. In the time lapse $0 < t < t_p$, the inlet streamwise velocity profile follows one of the precedent functions. For times $t > t_p$ the inlet streamwise velocity is null ($u = 0.0$). The term t_p is the necessary time for a piston to travel the full stroke length at a mean piston velocity U_p which may be constant or time dependent $u_p(t)$. See Figure 4(b). At the same inlet boundary condition, the value of the other two velocity components are null ($v_{inlet} = 0.0$ and $w_{inlet} = 0.0$) and the inlet temperature is fixed at ambient temperature. The rest of the boundary conditions are considered like isothermal non-slip wall, with the exception of the upper wall, for which we have imposed a free sleep wall condition. As initial conditions, it is considered that all velocities are null in the entire domain, temperature and pressure have the ambient values.

D. Computational domain characteristics

The computational domain has the following dimensions: $7.35D_0 \times 5.61D_0 \times 6D_0$ (approximately 14.55 cm × 11.01 cm × 11.88 cm) in x, y, and z directions, respectively. This domain was discretized through a non-uniform grid distribution employing 209 × 137 × 109 nodes; therefore, the minimal and maximal grid spacing are the following: $\Delta x_{min} = 0.0115D_0$ (boundary layers), $\Delta x_{max} = 0.0431D_0$; $\Delta y_{min} = 0.0115D_0$ (upper boundary layer), $\Delta y_{min} = 0.0184D_0$ (nozzle wall), $\Delta y_{max} = 0.0576D_0$; $\Delta z_{min} = 0.0184D_0$ (nozzle wall), $\Delta z_{max} = 0.0576D_0$. See Figure 4(a). The resolution was obtained after a grid/results independent study with four different resolutions (from 1.6 to 4.5×10^6 of nodes). The computation time was 4.0 CPU hours for every non-dimensional time in a single processor computer.

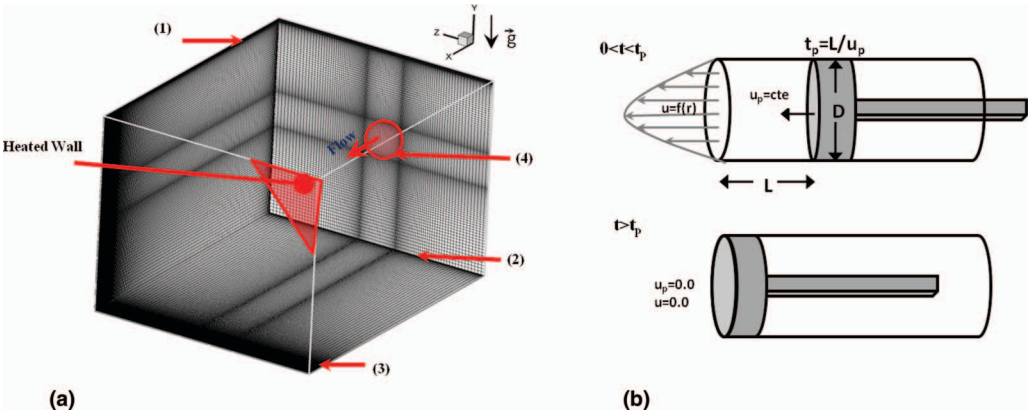

FIG. 4. Characteristics of the simulation: (a) Computational grid. Refinement zones: (1) up-wall, (2) inlet wall, (3) hot wall, and (4) nozzle wall; (b) inlet streamwise velocity treatment.

IV. FLOW PROPERTIES

A. Properties of the vortex rings

We carried out different measurements to analyze the vortex ring properties before the ring-wall head on collision. We conducted experiments for relatively small stroke ratios $L/D_0 \leq 3$. For the case of Newtonian flows,[27,33] single rings are formed for $L/D_0 \leq 4$ while for larger piston strokes, a leading vortex ring followed by a trailing jet and secondary vortices are observed. For such small stroke ratios, all the vorticity generated at the cylinder during liquid ejection is essentially entrained into the vortex ring leaving behind a calm flow;[28] in particular, the pinch-off process for $L/D_0 = 1$ is not-existent or insignificant. In Fig. 5(a), we show the vector field of a single vortex ring for $L/D_0 = 1$ and $Re = 2328$. For simplicity, the cylinder exit is placed at $x = 0$, so the vortex ring is located approximately at $x = 3D_0$. In order to compare the PIV measurements with the numerical simulations, we show in Fig. 5(b) velocity profiles of the vortex ring at different distances from the wall. For this case, $L/D_0 = 1$ and $Re = 2328$. Symbols represent experimental measurements while lines correspond to numerical results. We observe good agreement between numerical and experimental results. In particular, we observe that the vortex velocity at the center line ($y = 0$) evolves during vortex motion; particularly, for this piston stroke, the vortex velocity stabilizes approximately at $x = 3D_0$.

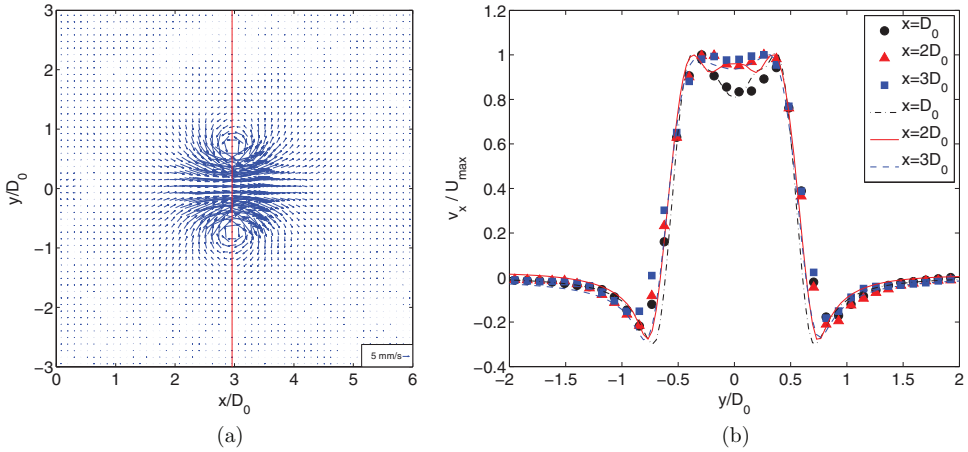

FIG. 5. (a) Velocity field obtained from PIV measurements, vortex is located at $x/D_0 \approx 3$; in this case the tube exit is located at $x = 0$. (b) Vortex velocity profiles at different distances from the wall; symbols represent experimental measurements while lines correspond to numerical results.

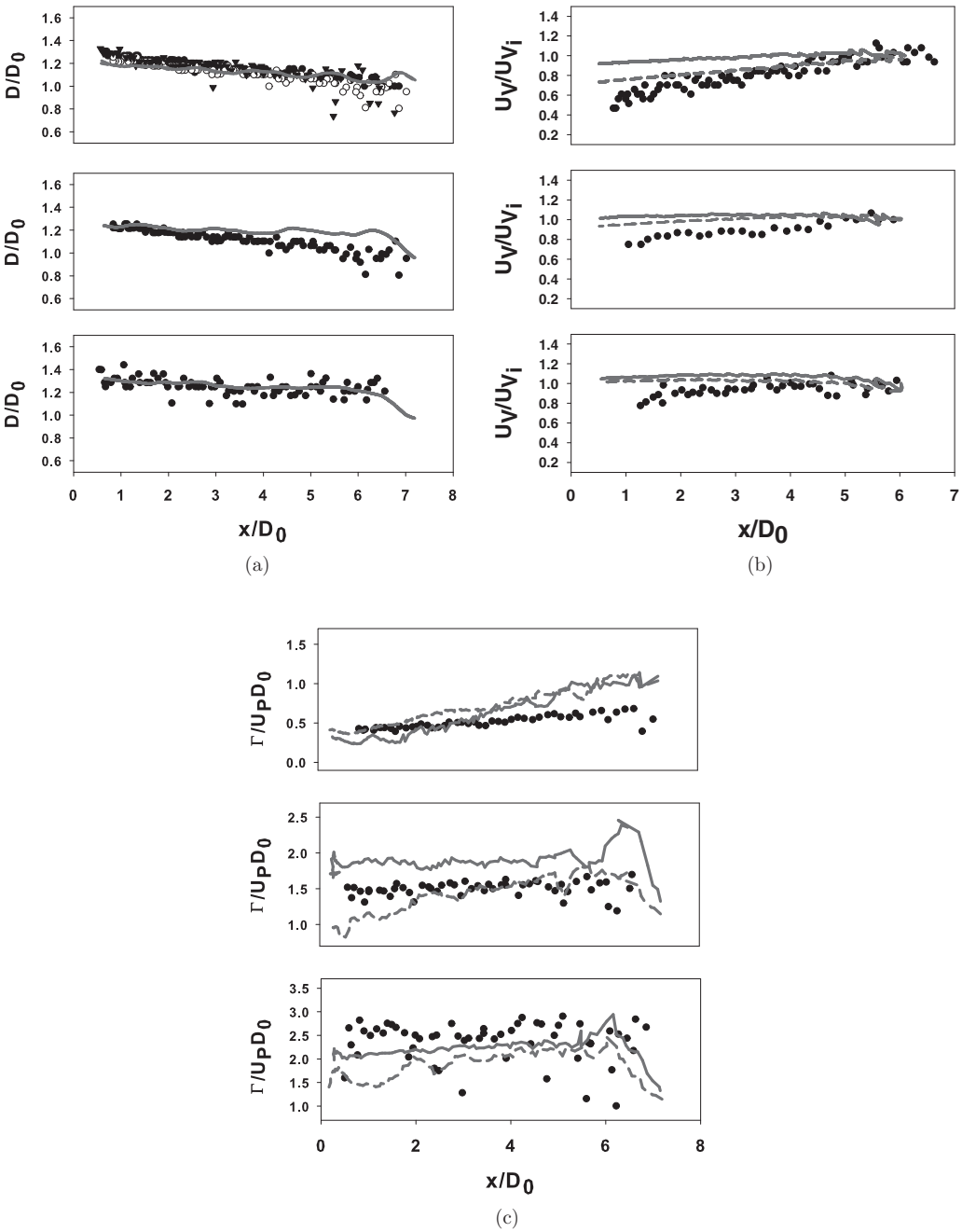

FIG. 6. Different vortex ring properties for $L/D_0 = 1, 2, 3$ (from top to bottom row) and $Re = 2910$ before wall collision: (a) diameter, (b) translation velocity, (c) circulation. Filled symbols: experimental data. Lines: numerical results, parabolic profile (continuous), turbulent profile (dashed).

In Figure 6, we present the vortex (a) diameter, (b) propagation velocity, and (c) circulation for three different stroke ratios: $L/D_0 = 1, 2, 3$ (from top to bottom row). The black points represent experimental results, the continuous lines represent numerical results for a starting jet with a flat turbulent profile (Eq. (11)) while the dashed lines represent results for the parabolic velocity profile (Eq. (12)). In all cases, the maximum piston velocity is $U_{p,\,max} = 15$ cm/s, so the Reynolds number is $Re = 2910$. The wall is located at $x = 0$ and the distance to the tube exit is about $x \approx 7D_0$.

The vortex ring radius R_v is defined as the distance between the axis of symmetry and the vortex core center. Therefore, the vortex diameter $D_v = 2R_v$ corresponds to the diameter of the self-rotation axis (azimuthal component ϕ) of the vortex ring.[15] In a 2D PIV vector field (vertical slice), the diameter is obtained by measuring of the distance between the geometrical centers of the upper and lower half section of the vortex ring using peak curvature (Eq. (2)). Some authors have defined the vortex diameter as the distance between vorticity peaks; however, these points do not necessarily coincide with the geometrical center. Palacios-Morales and Zenit[33] reported that the point of maximum vorticity in vortex rings tends to move towards the axial axis. In Fig. 6(a), we present the vortex diameter for different L/D_0; we observe that the vortex increases in size as it travels from the tube exit. The diameter increases slightly with the stroke ratio as well; this dependence of ring diameter on the stroke ratio has been reported by Didden.[49] From Fig. 6(a), we observe a good agreement between our experimental and numerical results. We observe that the vortex diameter is in the range $D_v/D_0 = 1 - 1.2$ (1.94–2.33 cm).

Fig. 6(b) shows the propagation velocity of the vortex ring U_v; the velocity is scaled with the initial vortex velocity U_{vi}. For the experimental results, the velocity is obtained by a numerical differentiation of the vortex ring position based on the location of maximum curvature. The velocity decreases slightly as the vortex travels, which agrees with previous results;[50] however, for $L/D_0 = 2$ and 3 the velocity remains roughly constant in the distance between wall and tube. The trend of numerical simulations is similar; however, the velocity decays faster in experimental measurements.

The circulation is an important parameter for the characterization of a vortex since it provides information about the "strength of rotation" of the ring during formation and evolution. When increasing the stroke ratio the vortex ring is able to accumulate more vorticity in its core;[27,28] Gharib *et al.*[27] reported that the maximum circulation that a vortex ring can attain during formation occurs close to $L/D_0 = 4$. In Fig. 6(c), we show the vortex circulation scaled with the tube diameter D_0 and the mean piston velocity U_p obtained from Eq. (1). The vortex circulation is obtained from Eq. (4). We observe that the vortex circulation increases with L/D_0 as expected. Clearly, the circulation remains roughly constant along the travel distance. For large Reynolds number O(1000), the circulation reduces slowly with distance; however, for $L/D_0 = 1$ the reduction of vortex circulation (about 50% in experiments) is more noticeable.

B. Properties of the natural convective layer

To conduct the measurements of the ring-wall interaction, the vertical wall was first heated outside the tank until the desired temperature at the wall surface was achieved. Then, the heating box was gently placed into the water tank using vertical guides; this procedure avoids the water tank to warm up together with the heated wall before tests. Thus, the initial water temperature in the tank, was close to the room temperature (typically $T_{inf} \approx 20\,^{\circ}\mathrm{C}$). After some time the convective flow driven by the heated wall produce a main low-circulation pattern in the entire domain. From the PIV technique, we obtained the velocity fields of the entire domain and the velocity profiles of the boundary layer; the laser plane was aligned vertically with the tube center. We conducted measurements for $\Delta T = T_w - T_{inf} = 7.6, 12.8, 18\,^{\circ}\mathrm{C}$. We found that the circulation flow has a maximum velocity of about 0.7 mm/s for $\Delta T = 18\,^{\circ}\mathrm{C}$. The Grashof number of the system based on the height H of the vertical wall is

$$Gr = \frac{g\beta(T_w - T_{inf})H^3}{\nu^2} \approx 10^8, \tag{13}$$

where g is the gravitational acceleration, β and ν are the volumetric thermal expansion coefficient and the kinematic viscosity of the surrounding water. Bejan and Lage[51] showed that for $0.001 < Pr < 1000$ the criterion for transition from laminar to turbulent flow is $Gr_y \sim 10^9$. Therefore, the boundary layer obtained in our experimental setup is laminar and stable.

It is expected that because the wall is inserted into the tank, some disturbance will be present in it. In order to study the properties of the boundary layer and to know the time to reach steady state and therefore the time to develop a steady boundary layer, we conducted PIV measurements at the vicinity of the heated wall. The velocity profiles U_{sh} of the momentum boundary layer in the

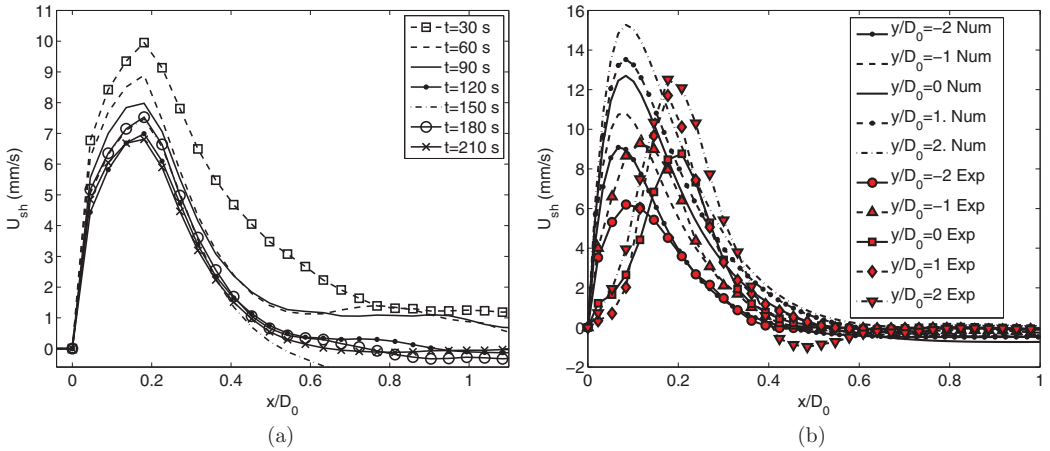

FIG. 7. Velocity profiles of the boundary layer. (a) Experimental profiles for $\Delta T = 12.8\,^{\circ}$C at different times after the heated wall is placed into the tank, $y = 0$. (b) Experimental and numerical profiles at different heights of the wall, $\Delta T = 18\,^{\circ}$C.

vertical direction (y axis) are presented in Fig. 7. In Fig. 7(a), we show the velocity profiles of the shear layer each 30 s after the heated wall is placed into the water tank for $\Delta T = 12.8\,^{\circ}$C. We show the profiles at $y = 0$ which coincides with the vortex ring axial axis. We observe that the maximum velocity decreases progressively until it reaches a constant value around $U_{sh,\,max} = 7$ mm/s and $U_{sh}(x \rightarrow \infty) \approx 0$. This condition was achieved in approximately 3 min for all cases. In Fig. 7(b), we show the experimental and numerical velocity profiles of the boundary layer at different heights of the wall for $\Delta T = 18\,^{\circ}$C. Measurements were taken 5 min after the heated wall was placed in the tank. In general, we observe that the boundary layer develops in the vertical direction; specifically, the boundary thickness δ and the maximum velocity $U_{sh,\,max}$ increase with y. For this case, the boundary thickness is about $\delta = 0.6D_0$ (11.6 mm). Similar characteristics were obtained for different wall temperatures ΔT. Comparing experimental and numerical results, we observe a slight difference on the peak velocity and thickness of the boundary layer.

C. Qualitative description of the vortex ring collision

In order to better describe the vortex-wall collision behavior, we first conducted ink visualization experiments. The pictures are shown in Figs. 8 and 9. The camera was placed either coaxial to the tube (frontal view) or perpendicular to it (side view). Pictures were taken at a sampling rate of 6 Hz using a CASIO EXILIM EX-F1 camera with 1920 × 1080 resolution. At the beginning of the experiment some ink is placed uniformly inside the tube close to the exit using a syringe. Considering reported values of water-soluble ink,[52] we infer the Schmidt number of the visualization, $Sc = \nu/D$ (where ν is the water kinematic viscosity and D is the ink diffusivity) to be of $O(10^2)$.

In Fig. 8, we show the side and frontal views of the ring-wall collision for the isothermal case (unheated wall): ink visualizations are presented in columns 1, 3 and concentration iso-surfaces (obtained from numerical simulations) in columns 2, 4. In this particular case $Re = 1940$ and $L/D_0 = 1$; the dimensionless times (from top to bottom row) are $t^* = 11.7$, 12.1, 13.6, and 16. From ink visualizations we first observe that the vortex diameter increases as it approaches the wall while the ring stretches in the azimuthal direction. For the isothermal case, we observe an axi-symmetric expansion during collision using different piston velocities and low piston strokes ($L/D < 2$). This behavior has been reported previously.[17,18] Columns 2 and 4 show passive scalar surfaces (concentration) with $C/C_{in} = 0.2$. The initial condition of the marker is similar to that of experiments: blue ink is placed at the edge of the nozzle. The mean velocity of the starting jet is very similar to that of the experimental mean piston velocity in order to obtain the same Reynolds number. Also, the times for the numerical result are approximately the same as those of the visualization sequence. We observe that the vortex diameter increases as the ring approaches the wall, as in

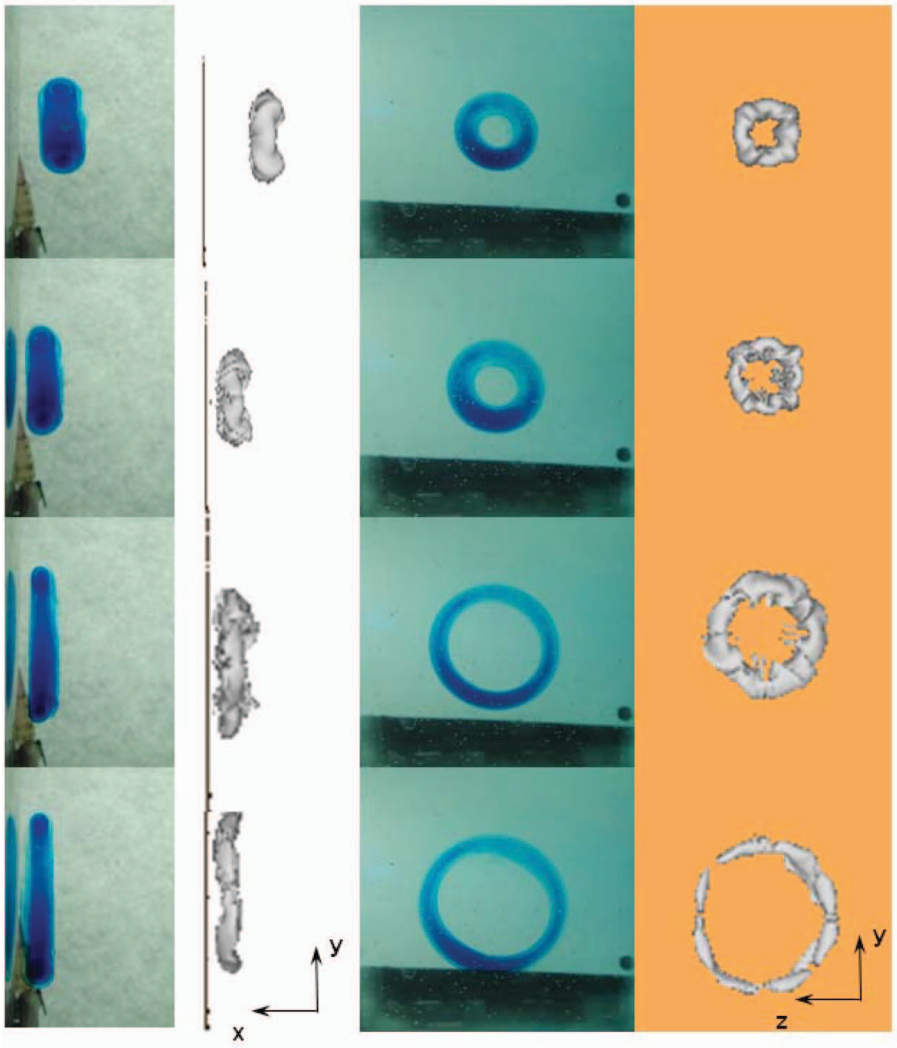

FIG. 8. Ring-wall collision, isothermal case: ink visualization (columns 1, 3) and concentration iso-surfaces (columns 2, 4) obtained from numerical simulations for $Re = 1940$ and $L/D_0 = 1$. Dimensionless times $t^* = 11.7$, 12.1, 13.6, and 16 (from top to bottom row).

the flow visualizations. The azimuthal axis of the ring remains parallel to the vertical wall during collision and the overall behavior of the vortex ring is essentially axially symmetric. It is important to note that for such small stroke ratio ($L/D_0 = 1$) it is difficult to observe from flow visualizations the production of secondary or tertiary vortices after a head on collision; however, secondary vortices are clearly observed in the PIV measurements and simulations, as we will show in Sec. V. When increasing the piston stroke, $L/D_0 \geq 2$, it is possible to observe from visualizations not only the formation of secondary vortices, but also the production of instabilities in the azimuthal direction which have been extensively reported by others.[17–21] Moreover, for relatively large piston strokes and high *Re* it is possible to observe experimentally the ejection of a new vortex ring from the wall as those reported by Walker *et al.*[17]

In Fig. 9, we show a sequence of images of a vortex ring colliding on the vertical wall for the same nominal condition as in Fig. 8 but for $\Delta T = 18\,^{\circ}\mathrm{C}$. The dimensionless times are $t^* = 11.7$, 12.1, 13.1, 15.5, and 17.5 (from top to bottom row). Similar to the isothermal case, we observe from ink visualizations that the vortex diameter increases as it approaches the wall; however, when reaching the thermal layer, the ring tilts with respect to the wall (towards the upstream direction). We observe that the upper section A stretches in the vertical direction and the ink diffuses with the

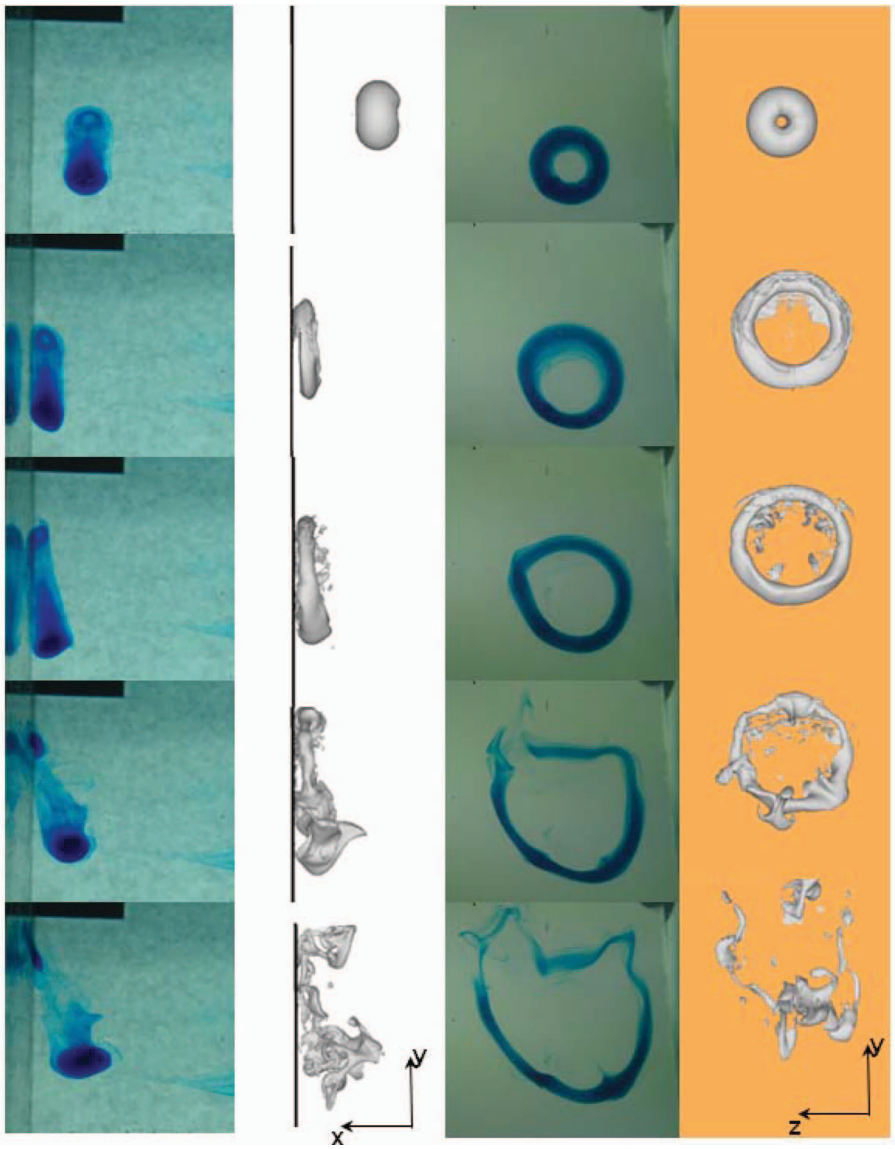

FIG. 9. Ring-wall collision, $\Delta T = 18\,^{\circ}\mathrm{C}$: ink visualisation (columns 1, 3) and concentration iso-surfaces (columns 2, 4) obtained from numerical simulations for $Re = 1940$ and $L/D_0 = 1$. Dimensionless times $t^* = 11.7$, 12.1, 13.1, 15.5, and 17.5 (from top to bottom row).

boundary flow. The lower section B "rebounds back" away from the wall but remains around the same vertical position. From the frontal view, we also note that the lateral sections of the vortex ring C and D move faster and stretch in the vertical direction. This stretching breaks the axisymmetry of the ring producing a "cat head" shape structure. This qualitative behavior was reproducible for all temperature differences studied here. In their experimental visualizations, Arévalo *et al.*[10] reported an asymmetric growth of the vortex ring after collision; they observed that the upper section moved faster than the lower section leading to a faster expansion along the vertical direction; they also observed that after collision, the remaining ring was convected away (moved upward) from the heater by entrainment of new hot fluid. However, they did not report the separation of the lower part of the ring from the wall; in our case, the bottom part of the ring was not convected away by the boundary layer after collision. In Fig. 9, we also show the evolution of the head-on collision obtained numerically. Likewise, the dimensionless times correspond to those of ink visualizations. We can observe in column 2 that the vortex ring tilts around the z axis as showed experimentally.

The lower section of the vortex ring separates from the wall while the upper section attaches to it ($t^* = 12.1$). We also observe that the upper and lateral sections stretch and diffuse faster than the lower section of the ring. Interestingly, we also observe from simulations that the largest concentration is located at the bottom section of the ring while the upper section diffuses faster.

Note also that the vortex ring behavior shown in Fig. 9 is very similar to that reported on vortex rings in crossflow.[22–25] In those cases, a vortex ring ejected normal to a cross flow tilts and deforms as it propagation in the flow direction. Particularly, the rotation has been observed in simple shear flows. The thickness of the ring becomes non-uniform as it propagates into the flow; Sau and Mahesh[23] attributed this deformation to the strain field experienced by the ring in crossflow while the tilting was attributed to the modification of the vorticity distribution of the ring as a result of the entrainment of background vorticity by the vortex core.[25] Clearly, the ratio of the initial vortex velocity to free-stream crossflow velocity and the stroke ratio determine the nature of deformation as well as the grade and direction of rotation.

V. RESULTS: RING-WALL INTERACTION

The collision behavior can change considerably depending on the vortex and thermal layer properties: L/D_0, Re, Gr, Pr, etc. For example, as we increase the piston velocity and stroke ratio (the vortex travel velocity and circulation are increased) we no longer observe the separation of the lower part of the ring from the wall; in fact, for large strokes ($L/D_0 = 4$) and high Re the vertical expansion is imperceptible. If the energy of the vortex ring (travel velocity and circulation) is similar to that of the boundary layer (maximum flow velocity and circulation), the latter can break the vortex symmetry in both the axial x and radial r directions. Moreover, if the thermal layer is strong enough, the entire vortex ring is convected away (moved upward) after vortex-wall interaction as observed by Ref. 10. We also observed that as we increase the stroke ratio and Re, flow instabilities emerge in the azimuthal direction making the description of the phenomenon even more complex. For all these reasons, we decided to focus our study to the case of $L/D_0 = 1$. This particular case has not been studied before. More importantly, it allow us to, first, study the vortex dynamics which will ultimately affect the rate of heat transfer.

In Fig. 10, we show the trajectories of the vortex centers (regions A and B, according to Fig. 1) for $Re = 2328$, $L/D_0 = 1$, and the temperature differences: (a) $\Delta T = 0$, (b) $\Delta T = 7.6\,^{\circ}\mathrm{C}$, (c) $\Delta T = 18\,^{\circ}\mathrm{C}$. To obtain the experimental trajectories, we first detected the vortex core using the Q criterion, then we computed the maximum curvature in the upper section A (black points) and lower section B (white points) of the vortex ring. The lines represent the results from numerical simulations. Only the trajectory of the primary vortex is plotted and the wall is placed at $x/D_0 = 0$. For the isothermal case, Fig. 10(a), we observe that the vortex centers separate as the ring approaches the wall as reported by several authors.[17,18] The behavior is roughly axi-symmetric. When the vertical wall is heated, Figs. 10(b) and 10(c), we observe that the upper section moves upward but remains at the same distance from the wall; the lower section separates from the wall and remains approximately at the same height from wall base. The numerical simulations agree well with experimental results; however, we noticed that for $\Delta T \neq 0$ the vortex ring does not always follow a straight trajectory; instead, it curves down slightly. Since the vortex velocity and strength are small, its trajectory may be affected by small remanent currents. Note that this deviation does not occur for $L/D_0 \geq 2$. Despite this small difference, both experiments and numerical results show that the vortex tilts when it interacts with the vertical current.

In Fig. 11, we show the evolution of the vorticity fields during vortex-wall collision for the case $L/D_0 = 1$, $\Delta T = 18\,^{\circ}\mathrm{C}$, and $Re = 2328$. The non-dimensional times are $t^* = 8.7$, 11.4, 14, and 16.6 (from top to bottom row). The left and right columns show the experimental and numerical results, respectively. At time $t^* = 8.7$ we show the vorticity field before collision. Near the wall, the vorticity of the thermal boundary layer can be observed; the vorticity has two signs, from positive (near the wall) to negative (in front of the ring). When the ring moves near the wall, the vorticity of the thermal layer increases.[18] At the time $t^* = 11.4$, we observe a strong interaction of the vorticity of the thermal layer with that of the vortex ring. First, the vorticity peak at the vortex core is increased,[20] the flow of the boundary layer is broken and the ejection (from the boundary layer) of a secondary vortex of

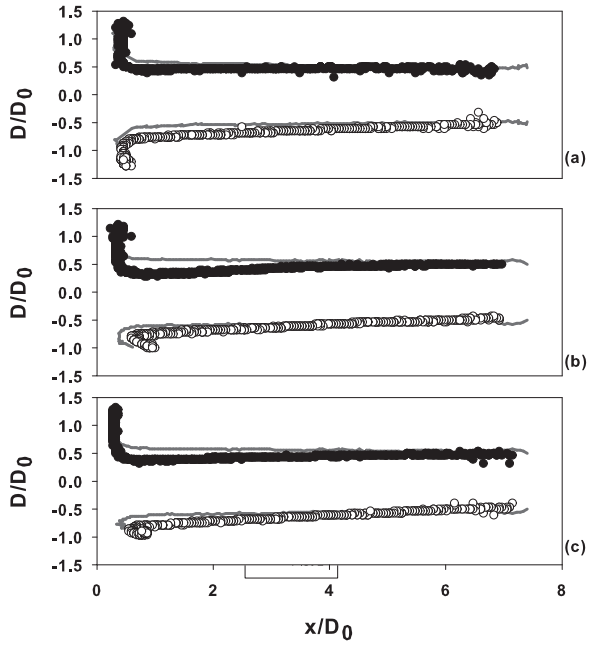

FIG. 10. Vortex trajectories for $Re = 2328$, $L/D_0 = 1$, and the temperature differences: (a) $\Delta T = 0$, (b) $\Delta T = 7.6\,^{\circ}\mathrm{C}$, (c) $\Delta T = 18\,^{\circ}\mathrm{C}$.

opposite whirl at the lower section is clearly observed. Smaller less perceptible secondary vortices are also formed at the upper section of the ring; however, it seems that they are not ejected away from the wall. Tertiary vortices are also observed in experiments and simulations at the ring lower section in time $t^* = 16.6$. As shown in the flow visualizations (Figs. 8 and 9) and the vortex center trajectories (Fig. 10), the vortex ring tilts forming an angle between the vortex plane (line between centers) and the vertical wall. The lower part rebounds back while the upper part attaches to the boundary layer. From Fig. 11 we also observe that the upper section of the ring seems to dissipate faster than the lower one, i.e., the circulation of the lower section is preserved for a longer time. After some time, the thermal boundary layer is restored and only the upper section of the ring is convected away.

To better quantify the vorticity change of both the upper and lower sections of the vortex ring during collision, we compute the circulation of the vortex core using Eq. (4). In Fig. 12, we show the experimental vortex circulation as a function of time for the upper (filled symbols) and lower (empty symbols) sections for $L/D_0 = 1$ and $Re = 2328$ for $\Delta T = 0$ and $\Delta T = 18\,^{\circ}\mathrm{C}$. In this figure, we plot the absolute value of the circulation, scaled with the tube diameter and piston velocity. The time is scaled with the tube diameter and the initial velocity of the vortex ring. For the isothermal case, we observe that the evolution of the vortex circulation of both ring sections is very similar. The vortex circulation decreases as the ring approaches the wall. The vortex-wall interaction starts at approximately $t^* = 10$; at this time, there is a slight increase of the vortex circulation which has been reported previously[20] as an increment of the maximum vorticity at the core center. Afterwards, the vortex circulation decrease occurs at a faster rate. For the case $\Delta T = 18\,^{\circ}\mathrm{C}$, we observe that the reduction rate of the vortex circulation is larger for the upper section of the ring. This is consistent with the vorticity fields shown in Fig. 11. It is important to note that the dissipation of vorticity resulting from the interaction with a wall is a process that is not well understood (see, for instance, Ref. 53). As shown below, by imposing a shear flow it is possible to significantly modify the rate of decay of circulation within the ring.

In Fig. 13, we show the circulation of the primary and secondary vortices obtained from numerical simulations for $L/D_0 = 1$ and $Re = 2328$ using Eq. (4), also for $\Delta T = 0$ and $\Delta T = 18\,^{\circ}\mathrm{C}$. The circulation is plotted the same way as in Fig. 12. We plot the circulation of regions A, B, C, and D, and also the angle between the wall and the ring plane. The vortex-boundary layer

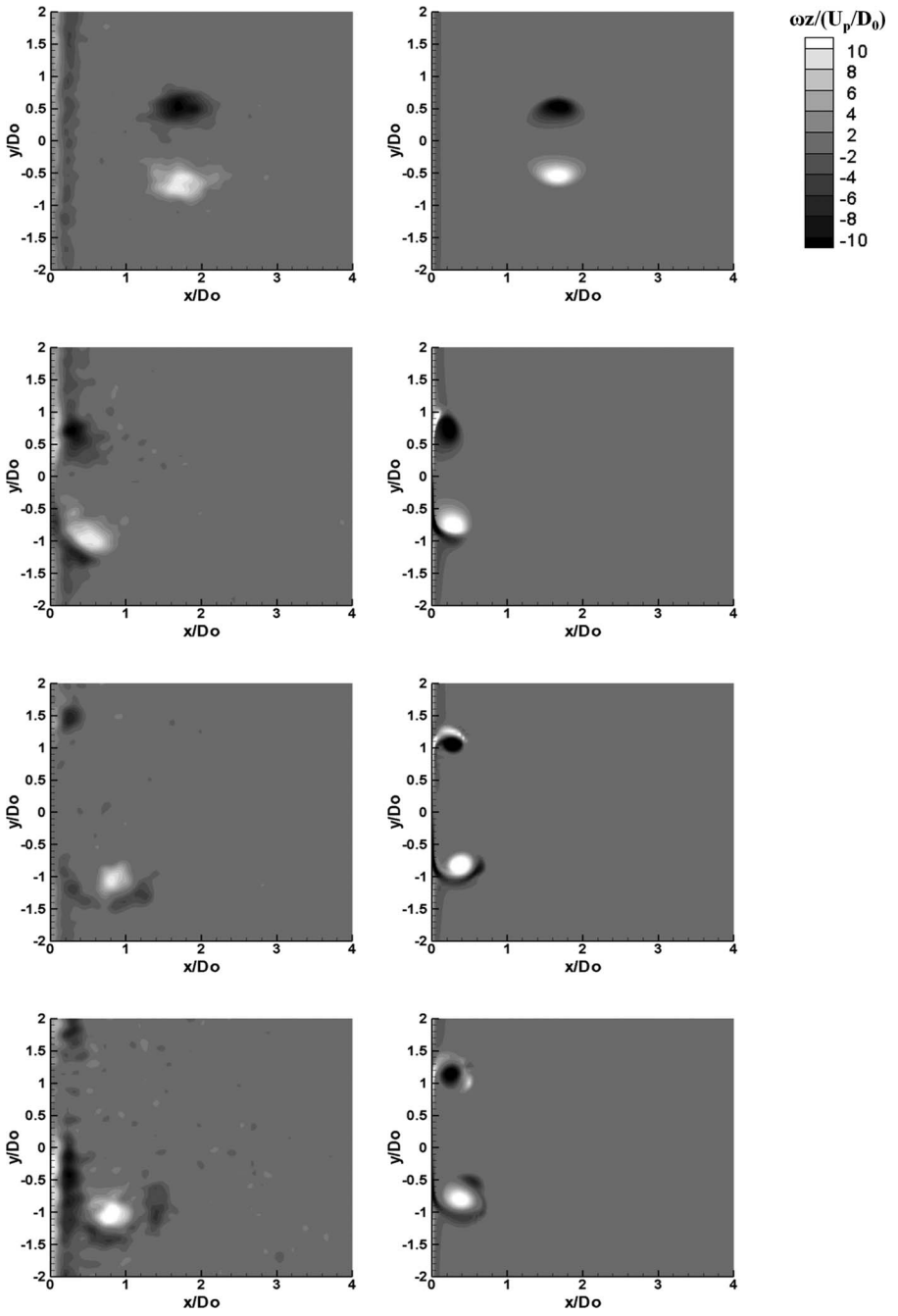

FIG. 11. Vorticity fields for $L/D_0 = 1$, $\Delta T = 18\,^{\circ}\mathrm{C}$, and $Re = 2328$. Times: $t^* = 8.7$, 11.4, 14, and 16.6 (from top to bottom row). Left column: experimental results. Right column: numerical results.

interaction starts at approximately $t^* = 8$ when a secondary vortex appears. For the isothermal case, we observe that the circulation evolution of the four sections of the primary and secondary vortices is essentially the same as expected. We also observe that the circulation of the primary vortex, in all sections, increases slightly just after the interaction starts, but decreases sharply in agreement with the experimental results. Since the wall is not heated, the vortex ring does not tilt during collision, thus the angle is always 0.

For the case $\Delta T = 18\,^{\circ}\mathrm{C}$, we observe that the reduction of circulation of the primary vortex is slower at the lower section of the ring (continuous line) as showed in experimental circulation results

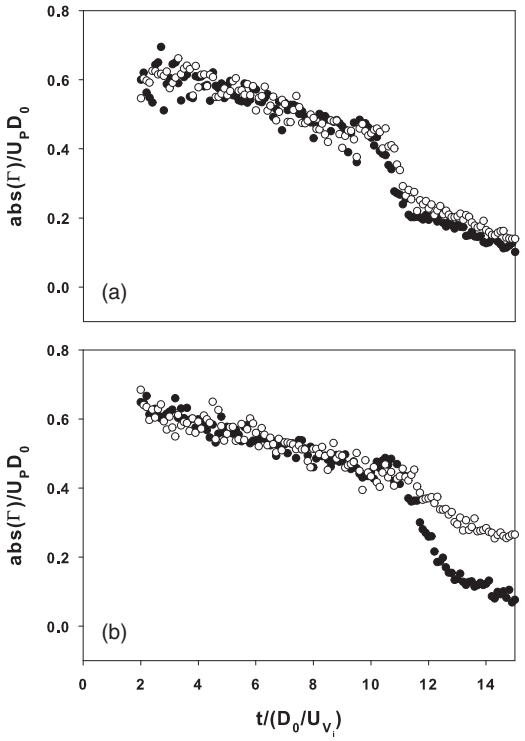

FIG. 12. Vortex circulation from experiments. (a) $\Delta T = 0$ and (b) $\Delta T = 18\,^{\circ}$C. $Re = 2328$ and $L/D_0 = 1$. Upper section A (filled symbols), lower section B (empty symbols).

in Fig. 12. On the other hand, the ring section that reduces faster its circulation is the upper one (dashed line). We also observe that the circulation of the secondary vortex increases significantly at the upper section just after ring-layer collision; however, the secondary vortex at the lower section obtains the largest circulation at $t^* = 10$. Again, this is consistent with the vorticity fields shown in Fig. 11 in which we observe that the secondary vortex generates strongly at the lower section of the ring. Since the upper section has vorticity sign equal to that of the outer section of the thermal boundary layer, the vortex circulation in this location increases rapidly; however, at the same time it dissipates faster than any of the other sections of the ring. Interestingly, the circulation of sections C and D seems to be unaffected by the interaction of the shear layer. For such regions, the vorticity of the ring is perpendicular to that of the thermal layer; hence, they interact only weakly. We also show the angle between the vortex plane and the vertical wall which first increases, then decreases at the same rate the circulation of the secondary vortex reduces and then the angle increases again to approximately 3°. Finally, in Fig. 13(c) we show the relation between the vortex circulation (primary vortex only) for the heated wall and isothermal cases $\Gamma_{\Delta T}/\Gamma_{\Delta T=0}$. Clearly, we observe that the vortex circulation of the primary ring at the bottom section is increased in the presence of the convective layer. On the contrary, the circulation of the primary vortex at the upper section is reduced when the wall is heated because faster viscosity dissipation.

A. Discussion

The main characteristics of the vortex ring-boundary layer interaction showed in our study are similar to experimental and numerical results reported by others. Sau and Mahesh[23] studied different conditions of vortex rings in crossflow varying the velocity ratio $r = U_{exit}/U_{flow}$ and the stroke ratio L/D_0, where U_{exit} and U_{flow} are the mean nozzle exit velocity and the free-stream velocity, respectively. For single vortex rings ($L/D_0 < 4$), they observed that the rings tilted towards the upstream direction if $2 \leq r \leq 10$. Cheng *et al.*[25] showed that a vortex ring generated in a simple

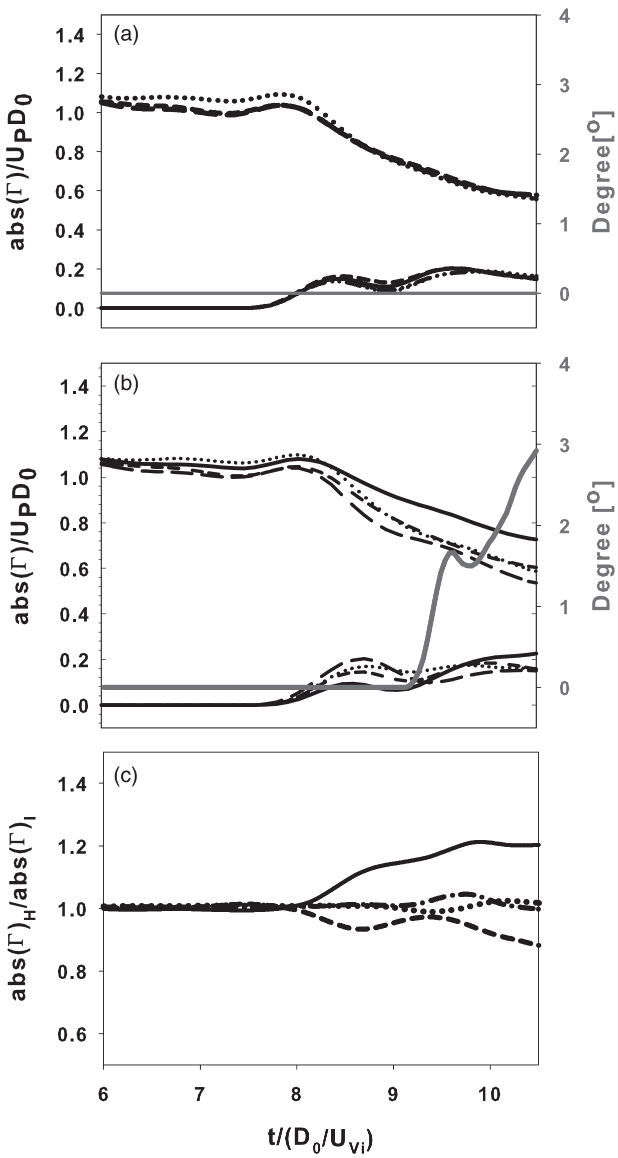

FIG. 13. Circulation of the primary and secondary vortices from numerical simulations. (a) $\Delta T = 0$ (b) $\Delta T = 18\,^{\circ}$C, (c) circulation ratio for the primary vortex $\Gamma_{\Delta T}/\Gamma_{\Delta T=0}$. Vortex sections: upper section A (- - - - -), lower section B (———), lateral section C (· · ·· ·· ·· ·· ·· ·· ·· ·· ·· · ·), and lateral section D (– – – – – -). Gray line represents the angle between the wall and the ring azimuthal plane.

shear flow will always tilt for vortex Reynolds number in the range $500 \leq Re_{\Gamma} \leq 1200$; the angle will grow progressively up to about 30°. It is important to note that in these cases the crossflow was first initiated before the generation of the ring; i.e., the vortex ring interacts with the crossflow at the same time it is forming and evolving. In our case, the vortex ring is fully formed in the fluid before the ring-crossflow interaction. However, qualitative similitude is remarkable. The recent numerical study of Guzmán *et al.*[26] is more similar to our case. They simulated the interaction of a vortex dipole with a sliding vertical wall; a shear layer was produced in the vicinity of the wall. They reported a "supercritical condition" for which only the vortex core with vorticity sign opposite to that of the shear layer (the bottom section in our case) separates from the wall and a secondary vortex of opposite whirl is also ejected away while the other core was convected by the shear layer. These conditions correspond to about $U_{wall}/U_{vortex} \geq 1.3$ where U_{wall} and U_{vortex} were the wall speed and dipole travel velocity, respectively.

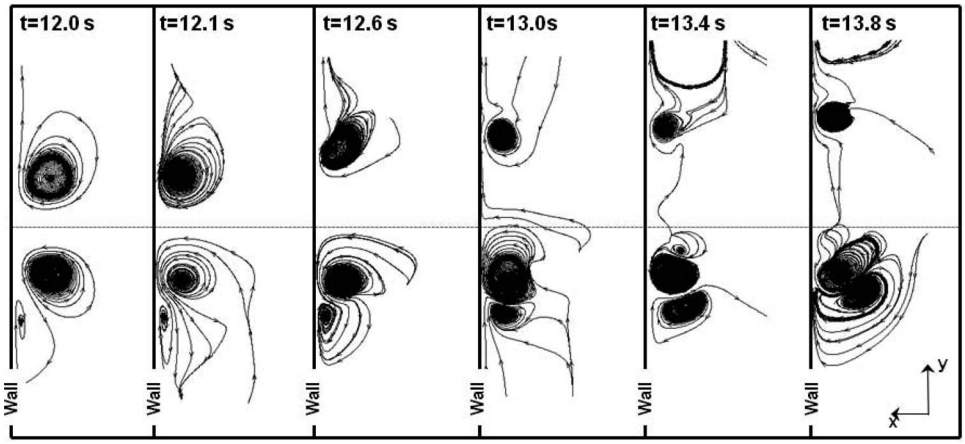

FIG. 14. Stream starches of the vortex ring during collision. $\Delta T = 40\,^{\circ}\mathrm{C}$.

In our experiment, we can define the velocity ratio $r = U_{vi}/U_{sh,max}$ where U_{vi} is the initial vortex velocity and $U_{sh,\,max}$ is the maximum velocity of the shear layer. For the particular case of $\Delta T = 18\,^{\circ}\mathrm{C}$, $L/D_0 = 1$, and $Re = 2328$, the initial vortex velocity is $U_{vi} \approx 20$ mm/s, and from Fig. 7, $U_{sh,\,max} \approx 9$ mm/s at $y = 0$; thus, $r = 2.2$. Considering this initial vortex velocity and the temperature range $\Delta T = 7.6 - 18\,^{\circ}\mathrm{C}$ we obtain $2.2 \leq r \leq 3.6$. According to Sau and Mahesh[23] the tilting of the vortex approaching the wall is expected in our study. For the experiments of Arévalo *et al.*,[10] $r \approx 3$; hence, some small tilting could be expected but was not reported or studied by the authors. We expect that as the velocity ratio r reduces the entire ring would be convected upwards by the shear layer, whereas if $r \gg 10$ the interaction between the vortex ring and the shear layer would be weak. It is also interesting to note that regions C and D seem to be unaffected by the interaction with the wall. These regions are merely convected by the flow. Since the vorticity in these regions is not in the same direction as that of the wall, a strong modification of the circulation is not expected.

In Fig. 14, we show stream traces of the vortex ring during collision. We can observe the initial process of boundary layer separation at both vortex cores[18] ($t = 12.1$ s) and the subsequent formation of a strong secondary vortex at the bottom part of the ring. On the contrary, at the upper section, a weaker primary vortex ring evolves during collision and is convected away by the thermal layer; no evidence of a secondary vortex ring at this region is observed. Evidently, the velocity of the shear layer must be large enough to inhibit the ejection of the vortex core.[26] From experimental (Fig. 12) and numerical (Fig. 13) results, we clearly observe that the circulation of the primary vortex (at the bottom section) after collision when the vertical wall is heated is larger compared to the isothermal case producing a wider ring (Fig. 14). Therefore, we can conclude that the vorticity of the primary and secondary vortex rings is increased at this section by the presence of the thermal boundary layer. The strong secondary vortex ring may promote the separation of the primary one from the wall as a result of a vortex pairing mechanism. Further investigation must be addressed to find different flow regimes; in particular, it would be interesting to study the vortex behavior in terms of the relation between the wall temperature and the vortex Reynolds number as well as the effect of the stroke ratio. We plan to pursue such an investigation in the future.

VI. CONCLUSIONS

A vortex ring impacting on a vertical heated wall was investigated considering experiments and numerical simulations. A TR-PIV system was used to measure the vorticity field and circulation in the vortex core during head on collision. A 3D numerical model was used to simulate the same experimental conditions. The dynamics of the interaction between the thermal boundary layer and the vortex ring was also studied. To better understand the interaction process, the behaviour of four separate ring sections was analyzed in time. Our results show that there is rich dynamic process: an asymmetric expansion and tilt are observed when then ring reaches the shear layer produced by the heated wall for $L/D_0 = 1$ and Re of O(1000). For these experimental conditions, the thermal layer

breaks and the vortex ring tilts slightly forming an angle between the wall and the ring (azimuthal) plane. The lower section of the vortex ring separates from the wall while the upper section remains close to the wall and is convected by the thermal layer; the lateral sections of the ring stretch faster producing a vertical expansion of the ring. Since the sign of vorticity of the upper section is the same as the vorticity sign of the outer region of the boundary layer, the maximum vorticity at the upper core increases at the beginning; however, this section dissipates faster than the lower one. The computation of the vortex core circulation indicates that the lower section of the ring reduces its circulation slower than any of the ring sections. In fact, stronger secondary vortices are formed at this location; therefore, the momentum transport and rate of heat transfer at this location should be the largest.

The results presented in this paper suggest, first, that the properties of the thermal layer and vortex ring determine the overall behavior of the ring-boundary layer interaction, the momentum transport from the boundary layer to the surroundings, and the resulting heat transfer. Second, the heat transfer along the vortex ring is not necessarily a symmetric process, instead, the local heat transfer will depend on the ring-boundary relative position and the structure of the surrounding flow. We plan to continue with the analysis of the heat transfer that results from this flow; we will report such results elsewhere.

ACKNOWLEDGMENTS

We are grateful to the Dirección General de Asuntos del Personal Académico for granting C. Palacios postdoctoral scholarship. The financial support to this project from PAPIIT (Grant No. IN115812) is also greatly appreciated. This work has been supported by CONACYT-Mexico-102527 (R. Zenit).

[1] D. R. Sabatino and C. R. Smith, "Turbulent spot flow topology and mechanisms for surface heat transfer," J. Fluid Mech. **612**, 81 (2008).
[2] A. R. Gifford, T. E. Diller, and P. P. Vlachos, "The physical mechanism of heat transfer augmentation in stagnating flows subject to freestream turbulence," J. Heat Transfer **133**(2), 021901 (2011).
[3] J. Jiménez, G. Kawahara, M. Simens, and J. del Alamo, "The near-wall structures of turbulent wall flows," in *Proceedings of the IUTAM Symposium on Elementary Vortices and Coherent Structures: Significance in Turbulent Dynamics* (Springer, Netherlands, 2006).
[4] A. Jacobi and R. Shah, "Heat transfer surfaces enhancement through the use of longitudinal vortices: A review of recent progress," Exp. Therm. Fluid Sci. **11**, 295 (1995).
[5] M. Fiebig, "Vortices and heat transfer," Z. Angew. Math. Mech. **77**, 3 (1997).
[6] A. Valencia and M. Sen, "Unsteady flow and heat transfer in plane channels with spatially periodic vortex generators," Int. J. Heat Mass Transfer **46**, 3189 (2003).
[7] S. J. Yang, "Numerical study of heat transfer enhancement in a channel flow using an oscillating vortex generator," Heat Mass Transfer **39**, 257 (2003).
[8] R. Romero-Méndez, M. Sen, K. T. Yang, and R. L. McClain, "Enhancement of heat transfer in an inviscid-flow thermal boundary layer due to a Rankine vortex," Int. J. Heat Mass Transfer **41**, 3829 (1998).
[9] R. Martin and R. Zenit, "Heat transfer resulting from the interaction of a vortex pair with a heated wall," Trans. ASME J. Heat Transfer **130**(5), 051701 (2008).
[10] G. Arévalo, R. H. Hernández, C. Nicot, and F. Plaza, "Vortex ring head-on collision with a heated vertical plate," Phys. Fluids **19**, 083603 (2007).
[11] G. Arévalo, R. H. Hernández, C. Nicot, and F. Plaza, "Particle image velocimetry measurements of vortex rings head-on collision with a heated vertical plate," Phys. Fluids **22**, 053604 (2010).
[12] D. O. Hubble, P. P. Vlachos, and T. E. Diller, "The role of large-scale vortical structures in transient convective heat transfer augmentation," J. Fluid Mech. **718**, 89 (2013).
[13] K. Shariff and A. Leonard, "Vortex rings," Annu. Rev. Fluid Mech. **24**, 235 (1992).
[14] T. T. Lim, and T. B. Nickels, "Vortex rings," *Fluid Vortices* (Kluwer, Dordrecht, 1995).
[15] D. G. Akhmetov, *Vortex Rings* (Springer, Berlin, 2009).
[16] T. L. Doligalski, C. R. Smith, and J. D. A. Walker, "Vortex interactions with walls," Annu. Rev. Fluid Mech. **26**(1), 573 (1994).
[17] J. D. Walker, C. R. Smith, A. W. Cerra, and T. L. Doligalski, "The impact of a vortex ring on a wall," J. Fluid Mech. **181**, 99 (1987).
[18] P. Orlandi and R. Verzicco, "Vortex rings impinging on walls: Axisymmetric and three-dimensional simulations," J. Fluid Mech. **256**, 615 (1993).
[19] C. Chu, C. Wang, and C. Chang, "A vortex ring impinging on a solid surface: Vortex structure and surface force," Phys. Fluids **7**, 1391 (1995).
[20] D. Fabris, D. Liepmann, and D. Marcus, "Quantitative experimental and numerical investigation of a vortex ring impinging on a wall," Phys. Fluids **8**, 2640 (1996).

[21] A. Naguib and M. Koochesfahani, "On wall-pressure sources associated with the unsteady separation in a vortex-ring/wall interaction," Phys. Fluids **16**, 2613 (2004).
[22] Y. K. Chang and A. D. Vakili, "Dynamics of vortex rings in cross-flow," Phys. Fluids **7**, 1583 (1995).
[23] R. Sau and K. Mahesh, "Dynamics and mixing of vortex rings in crossflow," J. Fluid Mech. **604**, 389 (2008).
[24] T. T. Lim, K. B. Lua, and K. Thet, "Does Kutta lift exist on a vortex ring in a uniform cross flow?," Phys. Fluids **20**, 051701 (2008).
[25] M. Cheng, J. Lou, and T. T. Lim, "Motion of a vortex ring in a simple shear flow," Phys. Fluids **21**, 081701 (2009).
[26] J. E. V. Guzmán, L. P. J. Kamp, and G. J. F. van Heijst, "Vortex dipole collision with a sliding wall," Fluid Dyn. Res. **45**(4), 045501 (2013).
[27] M. Gharib, E. Rambod, and K. Shariff, "A universal time scale for vortex ring formation," J. Fluid Mech. **360**, 121 (1998).
[28] M. Rosenfeld, E. Rambod, and M. Gharib, "Circulation and formation number of laminar vortex rings," J. Fluid Mech. **376**, 297 (1998).
[29] N. T. Oullette and J. P. Gollub, "Curvature fields, topology, and the dynamics of spatiotemporal chaos," Phys. Rev. Lett. **99**, 194502 (2007).
[30] W. Braun, F. de Lillo, and B. Eckhardt, "Geometry of particle paths in turbulent flows," J. Turbul. **7**, 62 (2006).
[31] G. Querzoli, M. Falchi, and G. P. Romano, "On the flow field generated by a gradually varying flow through an orifice," Eur. J. Mech. B/ Fluids **29**, 259 (2010).
[32] J. C. R. Hunt, A. Wray, and P. Moin, "Eddies, stream, and convergence zones in turbulent flows," Center for Turbulence Research Report CTR-S88, 1988.
[33] C. Palacios-Morales and R. Zenit, "Vortex ring formation for low Re numbers," Acta Mech. **224**, 383 (2013).
[34] C. Willert and M. Gharib, "Digital particle image velocimetry," Exps. Fluids **10**, 181 (1991).
[35] M. Raffel, C. Willert, and J. Kompenhans, *Particle Image Velocimetry: A Practical Guide* (Springer, Berlin, 1998).
[36] A. Sciacchitano, B. Wieneke, and F. Scarano, "PIV uncertainty quantification by image matching," Meas. Sci. Technol. **24**, 045302 (2013).
[37] J. J. Charonko and P. P. Vlachos, "Estimation of uncertainty bounds for individual particle image velocimetry measurements from cross-correlation peak ratio," Meas. Sci. Technol. **24**, 065301 (2013).
[38] M. Salinas-Vázquez and O. Métais, "Large-eddy simulation of the turbulent flow through a heated square duct," J. Fluid Mech. **453**, 201 (2002).
[39] A. J. Chorin, "A numerical method for solving incompressible viscous flow problems," J. Comput. Phys. **2**, 12 (1967).
[40] A. Perrin and H. H. Hu, "An explicit finite-difference scheme for simulation of moving particles," J. Comput. Phys. **212**(1), 166 (2006).
[41] M. Lesieur and O. Métais, "New trends in large eddy simulations of turbulence," Annu. Rev. Fluid Mech. **28**, 45 (1996).
[42] E. David, "Modélisation des écoulements compressibles et hypersoniques: Une approche instationnaire," Ph.D. thesis, Institut National Polytechnique de Grenoble, France, 1993.
[43] D. Gottlieb and E. Turkel, "Dissipative two-four methods for time-dependent problems," Math. Comput. **30**, 703 (1976).
[44] M. Salinas-Vázquez, W. Vicente, E. Martínez, and E. Barrios, "Large eddy simulation of a confined square cavity with natural convection based on compressible flow equations," Int. J. Heat Fluid Flow **32**, 876 (2011).
[45] M. Salinas-Vázquez, M. A. de la Lama, W. Vicente, and E. Martínez, "Large eddy simulation of a flow through circular tube bundle," Appl. Math. Model. **35**, 4393 (2011).
[46] T. J. Poinsot and S. K. Lelef, "Boundary conditions for direct simulations of compressible viscous flows," J. Comput. Phys. **101**, 104 (1992).
[47] K. Mohseni, H. Ran, and T. Colonius, "Numerical experiments on vortex ring formation," J. Fluid Mech. **430**, 267 (2001).
[48] H. Schlichting, *Boundary-layer Theory*, 7th ed. (McGraw-Hill, New York, 1979).
[49] N. Didden, "On the formation of vortex rings: Rolling-up and production of circulation," Z. Angew. Mech. Phys. **30**, 101 (1979).
[50] A. Weigand and M. Gharib, "On the evolution of laminar vortex rings," Exp. Fluids **22**, 447 (1997).
[51] A. Bejan and J. L. Lage, "The Prandtl number effect on the transition in natural convection along a vertical surface," Trans. ASME J. Heat Trans. **112**, 787 (1990).
[52] S. Lee, H.-Y. Lee, I.-F. Lee, and C.-Y. Tseng, "Ink diffusion in water," Eur. J. Phys. **25**, 331 (2004).
[53] K. C. Stewart, C. L. Niebel, S. Jung, and P. P. Vlachos, "The decay of confined vortex rings," Exp. Fluids **53**, 163 (2012).